Author Manuscript

Author Manuscript

Author Manuscript

Author Manuscript

HHS Public Access

Author manuscript

IEEE Trans Biomed Eng. Author manuscript; available in PMC 2018 October 01.

Published in final edited form as:

IEEE Trans Biomed Eng. 2018 October ; 65(10): 2136–2142. doi:10.1109/TBME.2017.2706976.

Monitoring acute stroke in mouse model using laser speckle imaging-guided visible-light optical coherence tomography

Qi Liu[†],
School of Biomedical Engineering, Shanghai Jiao Tong University, Shanghai, 20030, China and the Biomedical Engineering Department, Northwestern University, Evanston, Illinois, 60208, USA

Siyu Chen[†],
Biomedical Engineering Department, Northwestern University, Evanston, Illinois, 60208, USA

Brian Soetikno,
Biomedical Engineering Department, Northwestern University, Evanston, Illinois, 60208, USA

Wenzhong Liu,
Wenzhong Liu is with Opticent Inc., Evanston IL, 60208, USA

Shanbao Tong, and
School of Biomedical Engineering and Med-X Research Institute, Shanghai Jiao Tong University, Shanghai, 200030, China

Hao F. Zhang
Biomedical Engineering Department, Northwestern University, Evanston, Illinois, 60208, USA (phone: 847-491-2946; fax: 847-491-4928)

Abstract

Objective—Monitoring hemodynamic and vascular changes in the acute stages of mouse stroke models is invaluable in studying ischemic stroke pathophysiology. However, there lacks a tool to simultaneously and dynamically investigate these changes.

Methods—We integrated laser speckle imaging (LSI) and visible-light optical coherence tomography (Vis-OCT) to reveal dynamic vascular responses in acute stages in the distal middle cerebral artery occlusion (dMCAO) model in rodents. LSI provides full-field, real-time imaging to guide Vis-OCT imaging and monitoring the dynamic cerebral blood flow (CBF). Vis-OCT offers depth-resolved angiography and oxygen saturation (sO_2) measurements.

Results—Our results showed detailed CBF and vasculature changes before, during, and after dMCAO. After dMCAO, we observed insignificant sO_2 variation in arteries and arterioles and location–dependent sO_2 drop in veins and venules. We observed that higher branch-order veins had larger drops in sO_2 at the reperfusion stage after dMCAO.

Conclusion—This work suggests that integrated LSI and Vis-OCT is a promising tool for investigating ischemic stroke in mouse models.

Correspondence to: Shanbao Tong; Hao F. Zhang.

[†]Both authors contributed equally to this work.

Author Manuscript Author Manuscript Author Manuscript Author Manuscript

Significance—For the first time, LSI and Vis-OCT are integrated to investigate ischemic strokes in rodent models.

Index Terms

Ischemic stroke; laser speckle imaging; optical coherence tomography

I. Introduction

Ischemic stroke is a leading cause of death and disability worldwide [1]. In humans, the majority of stroke lesions are located in the middle cerebral artery (MCA) innervated area [2]. Animal middle cerebral artery occlusion (MCAO) models are widely used to study the physiology and pathology of ischemic stroke [3, 4]. Among these models, the distal middle cerebral artery occlusion (dMCAO) model in mouse is favored by many researchers because it mimics a major mechanism of cortical strokes in humans, thereby providing an ideal model to study focal ischemia on cerebral cortex [2].

Adequate cerebral blood flow (CBF), complete vasculature, and sufficient oxygen delivery are vital for brain to maintain normal functionality [5, 6]. During ischemic stroke, the perturbed vascular morphology causes abnormal blood flow and reduction of tissue oxygenation, thereby impairing brain's normal function [7]. Monitoring the changes of these parameters are important in understanding the pathological mechanisms of ischemic stroke [8, 9]. Moreover, measuring these pathophysiological parameters with high resolution during ischemic stroke is very helpful to reveal detailed hemodynamic changes, providing guidance for more effective timing of medical intervention [10]. However, simultaneously and dynamically measuring these parameters is difficult due to lack of effective tools.

Traditional imaging modalities such as functional magnetic resonance imaging (fMRI) [11] and positron emission tomography (PET) [12] have insufficient spatial and temporal resolution to resolve dynamic vascular responses. Optical imaging techniques are well suited to image changes in CBF, vascular morphology, and blood oxygenation thanks to their relative high imaging resolution and the distinct optical absorption properties of oxygenated and deoxygenated blood. Various optical techniques have been developed to measure these parameters. Nevertheless, acquiring all of these parameters using a single technique remains challenging. For example, laser Doppler imaging (LDI) [13] can measure blood flow, but has to compromise between the spatial and temporal resolution. Laser speckle imaging (LSI) [14] and optical intrinsic signal imaging (OIS) [15] are both full-field imaging techniques and can rapidly measure blood flow and blood oxygenation, respectively. However, they both lack depth-resolution, which reduces the imaging sensitivity and tends to bias the results. Two-photon microscopy (2PM) [16] yields information about vascular morphology and flow but it requires exogenous contrast agents. Photoacoustic microscopy (PAM) [17] can measure these parameters; however, it requires physical contact with the object. Optical coherence tomography (OCT) is capable to resolve 3D structural information [18]. However, the later three techniques are laser-scanning based, which limits their respective field-of-view and achievable frame-rate, making real-time observation of a larger area challenging.

Author Manuscript Author Manuscript Author Manuscript Author Manuscript

Combining multiple modalities (e.g. the full-field imaging techniques and the laser-scanning techniques) would potentially offer a good solution to the above challenges. For example, the combination of a LSI-based technique referred to as multi-exposure speckle imaging (MESI) and 2PM has been proposed to longitudinally study the neurovascular outcomes after ischemic stroke in mouse brain [19]. The combination of LSI and PAM has also been used to measure multiple hemodynamic parameters in acute ischemic injury in rat brain [20]. But they are still limited by introducing exogenous contrast agents for 2PM and the physical coupling between the sample the detector for PAM. The combination of LSI and OCT would not have such restrictions and would enable dynamic label-free measurement of neurovascular responses in stroke study with minimum perturbation. Recently, Dziennis et al. integrated a dual-wavelength laser speckle contrast imaging (2-LSI) system [21] and an optical microangiography (OMAG) system [22] to simultaneously measure these parameters before and after ischemic stroke [23]. However, the 2-LSI system increases the system complexity and cannot provide the blood oxygenation changes in depth-resolved blood vessels.

In this study, we integrated LSI and visible-light optical coherence tomography (Vis-OCT) to measure changes in CBF, vascular morphology and sO_2 before and after dMCAO. Vis-OCT [24] builds on OCT angiography (OCTA) [25] and spectroscopic OCT [26, 27]. It is capable of imaging sO_2 and has been demonstrated as a promising tool in cortical imaging [28, 29]. LSI was used to confirm the occlusion of blood vessels. LSI also guided Vis-OCT to locate the area of interest (AOI) and synchronized Vis-OCT imaging. Vis-OCT yielded the depth-coded angiography and sO_2 measurement at the capillary level. By combining LSI and Vis-OCT, we were able to characterize the dynamic changes in acute stages of dMCAO stroke model.

II. Methods and materials

A. Animal preparation

All the experimental protocols in this study have been approved by the Northwestern University Institutional Animal Care and Use Committee (NUIACUC).

A C57BL/6 mouse (23 g) was anesthetized with a mixture of isoflurane (4% for induction and 1.5% for maintaining) and air. The body temperature of the mouse was maintained at ~37°C with a heating pad and a DC module with feedback control (FHC, Stoelting Co.). To ease inflammation and swelling, dexamethasone (2.0 mg/kg body weight) was given subcutaneously before the craniotomy. After shaving the scalp, we applied lidocaine topically and made a midline scalp incision. The tissues underlying the scalp were cleaned to expose the skull. In order to reach the middle cerebral artery (MCA) before performing dMCAO, a 1-cm skin incision was made between the ear and eye. The temporal muscle was detached from the skull and the MCA was identified below the transparent skull. The bone above the artery was thinned until it was translucent and was withdrew to expose the MCA. After that, a square craniotomy window (4×4 mm^2) was made with a dental drill on the left cortex and the dura was left intact. A customized head holder was then laid on the skull with a 5×6 mm clearance above the monitoring window. Dental cement and solvent were applied around the head holder. The mouse was later transferred to a house-made animal

Author Manuscript Author Manuscript Author Manuscript Author Manuscript

holder for imaging. The head holder was clamped to a fixed stage which is connected to the animal holder to suppress motion artifacts.

In order to induce dMCAO, we used a bipolar forceps (Turtle, Germany), which is connected to a bipolar electro-surgical coagulator to block the artery by touching the exposed MCA on both sides. The LSI imaging will be continuously conducted throughout the entire dMCAO procedure. Vis-OCT imaging will be performed immediately before and after dMCAO, and up to 10 minutes after dMCAO.

B. Imaging system

Our experimental system consisted of two sub-systems: the LSI subsystem and the Vis-OCT subsystem (Fig. 1). For LSI, an uncollimated, unfocused laser beam (780 nm, 10 mW) was used to illuminate the cranial window. The scattered light was collected by an objective lens (LSM03-VIS, Thorlabs), and passed through the first lens element of a 4f telescope system, a dichroic mirror (FF654-SDi01, Semrock) and a long-pass filter (>750 nm, FEL0750, Thorlabs). The filtered lights were then captured by a CMOS camera (FMVU-03MTM, Pixelfly).

For Vis-OCT, we modified our previously reported free-space spectral-domain Vis-OCT system [28] by adding a 4f lens system in the sampling arm to accommodate the LSI light path. Briefly, a supercontinuum source (SuperK, NKT photonics) with a central wavelength of 566 nm and a bandwidth of 93 nm was used for illumination. The light was divided equally into both the sample arm and the reference arm by a cube beam splitter (CM1-BS013, Thorlabs). As indicated in Fig. 1, The OCT sampling arm shared the same objective as the LSI subsystem. We carefully matched the intensity and dispersive path length in the reference arm. The backscattered light from the sample arm and the reflected light from the reference arm were coupled and transmitted to a home-built spectrometer for the collection of interference spectrum from 513 nm to 620 nm using a line scan camera (spL2048-140km, Basler). The Vis-OCT provides lateral and axial resolutions of 11.9 μm and 1.2 μm (assuming the tissue refractive index is 1.37) in tissue, respectively.

C. CBF monitoring

LSI was used to continuously monitor the CBF before, during, and after the induction of dMCAO. The raw speckle images were continuously captured at 60 fps with an exposure time of 10 ms. The total time for CBF monitoring took ~9 minutes. For data processing, each 100 sequentially acquired images were used to calculate the CBF map. The speckle contrast value K at every pixel (i, j) was defined as

$$K = \frac{\sigma_{100}^{(i,j)}}{\mu_{100}^{(i,j)}}, \quad (1)$$

where σ_{100} and μ_{100} are the standard deviation and the average intensity at pixel (i, j) over 100 frames, respectively. In LSI [30], speckle contrast K is related to blood flow velocity v through correlation time τ_c (Eq. 2).

Author Manuscript Author Manuscript Author Manuscript Author Manuscript

$$K^2 = \beta\left[\frac{\tau_c}{T} + \frac{\tau_c^2}{2T^2}\left(e^{-\frac{2T}{\tau_c}} - 1\right)\right], \quad (2)$$

where T is exposure time; $\beta = 1/N$, and N is the number of speckles in each pixel area; τ_c is assumed to be inversely proportional to v [31]. We used $\frac{1}{K^2}$ in our study to represent relative blood flow velocity v at every pixel.

D. Vis-OCT angiography

Vis-OCT angiography was applied at three time points: before dMCAO, immediately after the MCA occlusion, and after the reperfusion of MCA branch. The MCA occlusion and the reperfusion of MCA branch were confirmed by real-time LSI. The Vis-OCT angiography imaging and processing protocols have been previously reported in [26]. Specifically, the Vis-OCT angiograph covered an area of 2.0×2.0 mm^2 and took 25.6 seconds.

III. Results

A. Real-time CBF mapping

We used LSI to continuously monitor the full-field CBF changes before, during, and after dMCAO. Fig. 2(a) shows LSI images at different time points. The LSI image at t = 0 min 0 sec was used as the reference image. We first attempted to induce dMCAO at t = 1 min 30 sec. Real-time LSI CBF map analysis immediately after the attempt revealed that MCA was not occluded successfully. We continuously monitored the CBF map for additional 1.5 minutes before our second attempt. The CBF map showed the dynamic changes of MCA branch, possibly due to normal vascular responses to the first occlusion attempt, though without occlusion. Specifically, at t = 2 min 22 sec, a MCA branch (M1) and its sub-branch were partially invisible in the CBF map. A few seconds later, these blood vessels reappeared in the CBF map. Another MCA branch, M2, also showed similar dynamic changes at t = 2 min 30 sec. The reappearances of the CBF in M1 and M2 indicated that the MCA was not yet occluded. We initiated a second dMCAO induction at t = 2 min 50 sec. The second induction of dMCAO took 3 seconds which was 50% longer than the first induction, increasing the chance of MCA occlusion. After the second attempt, we immediately checked the CBF map to determine if the MCA was occluded. The CBF map showed that MCA was totally occluded at 2 min 56 sec, as indicated by disappearance of the CBF in downstream vessels. It is worth noting that the downstream branch of M2 remained in the CBF map though the upstream has already been invisible. One minute after the MCA was occluded, the vasculature demonstrated dynamic changes. Comparing CBF maps at t = 2 min 56 sec and t = 3 min 58 sec, we found that some small blood vessels became visible as indicated by white arrows in Fig. 3(b). In addition to the recruitment of reserved small vessels, larger MCA branches also demonstrated dynamic changes in blood flow. At t = 4 min 15 sec, the previously occluded MCA was present in the CBF map. However, it only lasted for ~15s and then became invisible in the CBF map. The CBF of M1 and M2 gradually reappeared in the

Author Manuscript Author Manuscript Author Manuscript Author Manuscript

CBF map and remained visible. When the reperfusion of MCA branch became steady, we applied Vis-OCT again. CBF map at t = 7 min 47 sec shows when we were acquiring Vis-OCT image stacks.

We further analyzed the CBF changes in different vessels. In Fig. 2(b), we selected four blood vessels (F1–F4) as labeled in Fig. 2(a). The vertical axis represents the percentage of the baseline CBF level in the selected vessel areas. Before the first induction of dMCAO, CBF in the four vessels had few changes. Between the first induction and the second induction, the CBF value had dramatic fluctuation in selected areas and that is showed in the enlarged image on the upper right corner. After the first induction, V_{F1} increased to 105% of the baseline flow rate. Then it dropped to 25% and quickly rebounded to 95%. V_{F2} gradually decreased to 90% followed by a sudden decrease to 65%. After that, V_{F2} maintained at 65%. V_{F3} decreased to 95% followed by a sudden decrease to 60% and quickly rebounded to 95%. V_{F4} gradually decreased to 90%.

B. Vis-OCT angiography

We generated depth-coded angiography using Vis-OCT. It revealed morphological vascular changes during dMCAO. Fig. 3(a), Fig. 3(b), and Fig. 3(c) show the vascular network in the cortex before the induction of dMCAO, immediately after the MCA occlusion, and after the reperfusion of MCA branch, respectively. In the depth-coded map, the trunk of a pial vein lies closest to the surface while all other major blood vessels are within the superficial layers (<40 um). Arterioles, venules, and capillaries are in the deep layer. Immediately after dMCAO, capillaries, arterioles, and venules were not visible in ischemic core area (white dotted area). Though some MCA branches can still be identified in the angiography map (blue arrows), the CBF has significantly reduced (LSI image at t = 2 min 56 sec). It is noticed that in the area outside of ischemic core, new capillaries (white arrow) became visible immediately after the MCA occlusion. After the reperfusion of MCA branch, major branches of MCA and some small branches of pial vein are visible in the ischemic core. In the peripheral area, some of the newly recruited capillaries became invisible while others remained with minor changes in morphology. Despite vessel recruitment, the angiography map shows that overall capillaries density reduced immediately after the MCA occlusion. To further demonstrate dynamic changes in vascular structure, we took three angiographic B-scans, Fig. 3(d), Fig. 3(e), and Fig. 3(f) from the locations indicated by the white dashed line in Fig. 3(a). The comparison showed the decreased OCTA intensity on MCA branches immediately after MCA occlusion and the increased OCTA intensity after the reperfusion of MCA branch (red arrows).

C. Vis-OCT oximetry

To monitor blood oxygenation changes during dMCAO, we used the algorithms reported in [28] to calculate sO_2. Fig. 4 show the sO_2 map before the induction of dMCAO (Fig. 4(a)), immediately after the MCA occlusion (Fig. 4(b)), and after the reperfusion of MCA branch (Fig. 4(c)). Arteries and veins could be distinguished according to their measured sO_2 values in pseudocolors [29, 32], which agrees with morphology-based identifications.

Author Manuscript Author Manuscript Author Manuscript Author Manuscript

We calculated the mean sO_2 values on several blood vessels for comparison. The measured sO_2 (Mean±S.D) were plotted side-by-side in Fig. 4(d). We found that the measured sO_2 values in arteries changed little in all measurements. The sO_2 values in A3 were 86.6±3.6%, 85.3±4.9% and 85.7±4.1% at the three stages of experiment, respectively. Similarly, sO_2 values in A1 and A2 were 88.1±4.8% and 88.9±2.7% before the induction; and 88.4±6.5% and 89.9±6.3% after reperfusion of MCA branch, respectively. Note that sO_2 in A1 and A2 immediately after the occlusion were not available due to lack of OCTA contrast. On the contrary, the sO_2 values in veins and venules demonstrated greater variation during the period. We selected several branches of the imaged pial vein (V1 to V4) and another identified superficial vein (V5) to compare the sO_2 values. Notably, V2 and V3 lie on the border of the ischemic core, while V5 is far from it. Before the induction of dMCAO, all selected veins had similar sO_2 value of around ~76%. Immediately after the MCA occlusion sO_2 from V1 showed a ~3% decrease from 75.8±4.4% to 72.9±4.7%. V2 and V4 decreased significantly from 77.5±3.1% and 76.6±4.2% to 71.4±3.7 and 69.3±3.8%, respectively. Also, it is interesting that the sO_2 value in V5 (from 74.7±3.3% to 65.8±4.7%) has larger decease than both of that in V2 and V3. After the reperfusion of MCA branch, sO_2 value in V4 recovered to baseline level. In other veins, the sO_2 values were all decreased. When compared the sO_2 values before the dMCAO induction and after the reperfusion of MCA branch, we observed that higher order veins had larger decrease in sO_2 value in consecutive vein branches. The mean sO_2 values in V1, V2 and V3 decreased 2%, 12% and 14%, respectively.

IV. Discussions and conclusion

In this study, we integrated LSI and Vis-OCT to investigate the hemodynamic responses during the acute stages of dMCAO. LSI offered real-time imaging of dynamic changes of blood flow and corresponding CBF map, which guided the timing and location (field-of-view or FOV) selection for Vis-OCT. Vis-OCT provided depth-resolved angiography and sO_2 map in the FOV at the selected time.

In our dMCAO experiments, we observed the reperfusion of MCA branch 1 minute 12 seconds after dMCAO and it was confirmed by both LSI CBF map and Vis-OCT angiography. Other groups also reported similar observations [23, 33]. The blood flow compensated for by the anterior cerebral artery (ACA) was assumed to be the main mechanism. ACA is considered the salvage artery in MCA supplied areas when ischemia occurs [23]. The downstream branch of M2 was present even though the upstream of this arteriole had no flow after the MCA occlusion. This phenomenon may be attributed to the reverse flow from communicating arterioles between parallel MCA branches on cortical surface [33] or from anastomoses between ACA and MCA [23]. The blood flow in M1 and M2 changed dramatically between the first induction and the second induction of dMCAO though MCA was not occluded. This might be due to the influence exert by the intravascular thrombus which was formed during the first coagulation [34]. The thrombus consisted of platelet aggregates could be generated and affect the blood flow along vessel direction [35, 36]. Since the MCA was not occluded and the blood continued to flow, it is likely that the generated thrombus may be flushed to M1 and M2 and disturbed the blood flow.

Author Manuscript Author Manuscript Author Manuscript Author Manuscript

Immediately after dMCAO, we found new capillaries from Vis-OCT angiography map, which were not present before the induction of dMCAO. The minimum detectable velocity in our OCTA is at least 43 μm/s. Those capillaries may have lower velocity than the minimum detectable velocity before dMCAO, which cannot be detected by the current vis-OCT system. After the dMCAO, the velocity may increase in the vessel, making it detectable by vis-OCT. The appearance of these new capillaries may also indicate the existence of reserve capillary before the injury, which is known as capillary recruitment [37]. Some MCA branches can be found in Vis-OCT angiography map (indicated by blue arrows in Fig. 3(b)). However, LSI image showed no observable MCA branches at the same time (t = 2 min 56 sec). Though both LSI and Vis-OCT angiography are based on motion-enhanced contrast, Vis-OCT has mush higher axial resolution and higher sensitivity to lower blood flow than LSI. On the other hand, LSI has larger FOV to guide Vis-OCT to identify the desired FOV. LSI can also provide real-time monitoring of CBF and integrated vasculature changes while so far large FOV, real-time OCT imaging remains challenging, if not impossible. Currently, LSI is able to provide relative CBF changes in selected areas on superficial tissue layer. In the stroke study, monitoring the relative changes of CBF is important and useful. For example, in MCAO model, a drop of 70~80% of the baseline CBF on the surface of the ipsilateral dorsolateral cortex is a widely accepted criteria of a successful stroke [38] and the ischemic area with 50% reduction of the baseline CBF at the first minute after the stroke was correlated with the infarct volume at 24 hours after the stroke [39]. Indeed, LSI has been widely used in stroke study to monitor CBF changes before, during and after stroke [40]. All of these show the benefit of the combination of LSI and Vis-OCT.

In sO_2 measurement, we excluded the vessels in the ischemic core (white dotted area) immediately after the MCA occlusion. The reason is the greatly diminished Vis-OCT angiography intensity, which leads to incorrect sO_2 calculation. Immediately after the dMCAO, V5 had largest decrease in sO_2, which may be resulted from the penumbra area where the extraction of oxygen from blood was accelerated. After the reperfusion of MCA branch, the sO_2 value in V4 increased to the baseline level. The relative CBF value (Fig. 2(b)) also increased after the reperfusion of MCA branch when compared with the value after MCA occlusion. It is most likely that the reperfusion of MCA delivered oxygenated blood to V4. In regions where artery and vein overlapped, the measured sO_2 values were influenced by both arteries and veins are between the normal arteries and veins (dashed red circle in Fig. 4(a)). After the reperfusion of MCA branch, the sO_2 values in this area were the lowest (~50%) because only one vein branch left and the oxygen unloading from blood to tissue increased.

It should be noted that there is a resolution mismatch in our integrated system. The lateral resolution of LSI is around 8 μm and the lateral resolution of Vis-OCT imaging is around 12 μm. Considering the size of the overlapped image area (2.0×2.0 mm^2) in the LSI and Vis-OCT images, the maximum resolution mismatch (~4 μm) is considered negligible for co-registration of maps from the two modalities. To monitor the dynamics in small vessels, we needed to manually select the area inside the vessel. The minimum measurable diameter of the vessel is determined by LSI, which is around 32 μm. Even with the maximum resolution mismatch, the areas selected in LSI image and the corresponding Vis-OCT image could have

Author Manuscript Author Manuscript Author Manuscript Author Manuscript

an area mismatch around 1.5% which is almost negligible in measuring dynamics of the small vessels. Therefore, we think it will not affect the monitoring of the dynamics in small vessels and the co-registration of maps from the two modalities.

In summary, we have demonstrated the benefits of integrating LSI and Vis-OCT as an effective imaging platform to investigate multiple vascular changes after stroke. We showed the detailed CBF and vasculature changes before, during, and after dMCAO. The sO_2 values had little changes in arteries and arterioles after dMCAO induction; the sO_2 values decreased in veins and venules with different rates. In particular, higher order veins had larger decrease in sO_2 in consecutive vein branches after the reperfusion. We believe that this LSI-guided Vis-OCT system has broad application to study various vascular diseases.

Acknowledgments

This work was supported in part by the National Institute of Health grants R24EY022883, DP3DK108248 and R01EY026078, the National Science Foundation grants CBET-1055379 and DBI-1353952, the National Natural Science Foundation of China grant 61371018, and Chinese program of introducing talents to Universities (111 Project, No. B08020). Q. Liu is supported in part by the China Scholarship Council (201406230188).

References

1. Roger VL, et al. Heart disease and stroke statistics—2012 update a report from the American heart association. Circulation. 2012; 125(1):e2–e220. [PubMed: 22179539]
2. Llovera G, et al. Modeling stroke in mice: Permanent coagulation of the distal middle cerebral artery. JoVE (Journal of Visualized Experiments). 2014; 89:e51729–e51729.
3. Carmichael ST. Rodent models of focal stroke: size, mechanism, and purpose. NeuroRx. 2005; 2(3): 396–409. [PubMed: 16389304]
4. Howells DW, et al. Different strokes for different folks: the rich diversity of animal models of focal cerebral ischemia. Journal of Cerebral Blood Flow & Metabolism. 2010; 30(8):1412–1431. [PubMed: 20485296]
5. Dirnagl U, et al. Pathobiology of ischaemic stroke: an integrated view. Trends in neurosciences. 1999; 22(9):391–397. [PubMed: 10441299]
6. Pascarella L, et al. Microcirculation and venous ulcers: a review. Annals of vascular surgery. 2005; 19(6):921–927. [PubMed: 16247708]
7. Nishimura N, et al. Penetrating arterioles are a bottleneck in the perfusion of neocortex. Proceedings of the National Academy of Sciences. 2007; 104(1):365–370.
8. Agarwal S, et al. From Time is brain to Physiology is brain: a case for reflection in acute stroke treatment decisions. Brain. 2015; 138(7):1768–1770. [PubMed: 26106094]
9. Jackson SP. Arterial thrombosis—insidious, unpredictable and deadly. Nature Medicine. 2011; 17(11):1423–1436.
10. Hainsworth AH, Markus HS. Do in vivo experimental models reflect human cerebral small vessel disease? A systematic review. Journal of Cerebral Blood Flow And Metabolism. 2008; 28(12): 1877–1891. [PubMed: 18698331]
11. Ogawa S, et al. Functional brain mapping by blood oxygenation level-dependent contrast magnetic resonance imaging. A comparison of signal characteristics with a biophysical model. Biophysical journal. 1993; 64(3):803. [PubMed: 8386018]
12. Heiss WD, et al. Dynamic penumbra demonstrated by sequential multitracer PET after middle cerebral artery occlusion in cats. Journal of Cerebral Blood Flow & Metabolism. 1994; 14(6):892–902. [PubMed: 7929654]
13. Dirnagl U, et al. Continuous measurement of cerebral cortical blood flow by laser-Doppler flowmetry in a rat stroke model. Journal of Cerebral Blood Flow & Metabolism. 1989; 9(5):589–596. [PubMed: 2674168]

Author Manuscript Author Manuscript Author Manuscript Author Manuscript

14. Dunn AK, et al. Dynamic imaging of cerebral blood flow using laser speckle. Journal of Cerebral Blood Flow And Metabolism. 2001; 21(3):195–201. [PubMed: 11295873]
15. Grinvald A, et al. Functional architecture of cortex revealed by optical imaging of intrinsic signals. Nature. 1986; 324:361–364. [PubMed: 3785405]
16. Denk W, et al. Two-photon laser scanning fluorescence microscopy. Science. 1990; 248(4951):73–76. [PubMed: 2321027]
17. Zhang HF, et al. Functional photoacoustic microscopy for high-resolution and noninvasive in vivo imaging. Nature biotechnology. 2006; 24(7):848–851.
18. Huang D, et al. Optical coherence tomography. Science (New York, NY). 1991; 254(5035):1178.
19. Schrandt CJ, et al. Chronic monitoring of vascular progression after ischemic stroke using multiexposure speckle imaging and two-photon fluorescence microscopy. Journal of Cerebral Blood Flow & Metabolism. 2015; 35(6):933–942. [PubMed: 25712498]
20. Deng Z, et al. In vivo imaging of hemodynamics and oxygen metabolism in acute focal cerebral ischemic rats with laser speckle imaging and functional photoacoustic microscopy. Journal of biomedical optics. 2012; 17(8):0814151–0814159.
21. Qin J, et al. Fast synchronized dual-wavelength laser speckle imaging system for monitoring hemodynamic changes in a stroke mouse model. Optics letters. 2012; 37(19):4005–4007. [PubMed: 23027260]
22. Qin J, et al. Hemodynamic and morphological vasculature response to a burn monitored using a combined dual-wavelength laser speckle and optical microangiography imaging system. Biomedical optics express. 2012; 3(3):455–466. [PubMed: 22435094]
23. Dziennis S, et al. Macro-to-micro cortical vascular imaging underlies regional differences in ischemic brain. Scientific reports. 2015; 5:10051. [PubMed: 25941797]
24. Yi J, et al. In vivo functional microangiography by visible-light optical coherence tomography. Biomedical optics express. 2014; 5(10):3603–3612. [PubMed: 25360376]
25. Wang RK, et al. Three dimensional optical angiography. Optics Express. 2007; 15(7):4083–4097. [PubMed: 19532651]
26. Yi J, Li X. Estimation of oxygen saturation from erythrocytes by high-resolution spectroscopic optical coherence tomography. Optics letters. 2010; 35(12):2094–2096. [PubMed: 20548397]
27. Robles FE, et al. Assessing hemoglobin concentration using spectroscopic optical coherence tomography for feasibility of tissue diagnostics. Biomedical optics express. 2010; 1(1):310–317. [PubMed: 21258468]
28. Chen S, et al. Imaging hemodynamic response after ischemic stroke in mouse cortex using visible-light optical coherence tomography. Biomedical Optics Express. 2016; 7(9):3377–3389. [PubMed: 27699105]
29. Chong SP, et al. Cerebral metabolic rate of oxygen (CMRO 2) assessed by combined Doppler and spectroscopic OCT. Biomedical optics express. 2015; 6(10):3941–3951. [PubMed: 26504644]
30. Briers JD, Webster S. Laser speckle contrast analysis (LASCA): a nonscanning, full-field technique for monitoring capillary blood flow. Journal of Biomedical Optics. 1996; 1:174–179. [PubMed: 23014683]
31. Lemieux PA, Durian D. Investigating non-Gaussian scattering processes by using< i> n</i> th-order intensity correlation functions. Journal Of The Optical Society Of America A-optics Image Science and Vision. 1999; 16(7):1651–1664.
32. Ning B, et al. Ultrasound-aided multi-parametric photoacoustic microscopy of the mouse brain. Scientific reports. 2015; 5:18775. [PubMed: 26688368]
33. Schaffer CB, et al. Two-photon imaging of cortical surface microvessels reveals a robust redistribution in blood flow after vascular occlusion. Plos Biology. 2006; 4(2):e22. [PubMed: 16379497]
34. Kennedy J, et al. High-burst-strength, feedback-controlled bipolar vessel sealing. Surgical endoscopy. 1998; 12(6):876–878. [PubMed: 9602010]
35. Allan J, et al. Infrared evaluation of the heat-sink bipolar diathermy dissection technique. Journal of Plastic, Reconstructive & Aesthetic Surgery. 2015; 68(8):1145–1151.

Author Manuscript Author Manuscript Author Manuscript Author Manuscript

36. Livengood RH, , et al. SPIE BiOS. International Society for Optics and Photonics; 2011. Hyperthermic tissue sealing devices: A proposed histopathologic protocol for standardizing the evaluation of thermally sealed vessels; 79010Y–79010Y-9.

37. Parthasarathi K, Lipowsky HH. Capillary recruitment in response to tissue hypoxia and its dependence on red blood cell deformability. American Journal of Physiology-Heart and Circulatory Physiology. 1999; 277(6):H2145–H2157.

38. Peters O, et al. Increased formation of reactive oxygen species after permanent and reversible middle cerebral artery occlusion in the rat. Journal of Cerebral Blood Flow & Metabolism. 1998; 18(2):196–205. [PubMed: 9469163]

39. Li Y, et al. Predicting the ischemic infarct volume at the first minute after occlusion in rodent stroke model by laser speckle imaging of cerebral blood flow. Journal Of Biomedical Optics. 2013; 18(7):076024–076024.

40. Dunn AK. Laser Speckle Contrast Imaging of Cerebral Blood Flow. Annals of Biomedical Engineering. 2012:1–11. [PubMed: 22012081]

Appendix

The authors declare the following competing financial interest(s): Wenzhong Liu and Hao F. Zhang has financial interests in Opticent Inc. All remaining authors declare no competing financial interests.

Author Manuscript Author Manuscript Author Manuscript Author Manuscript

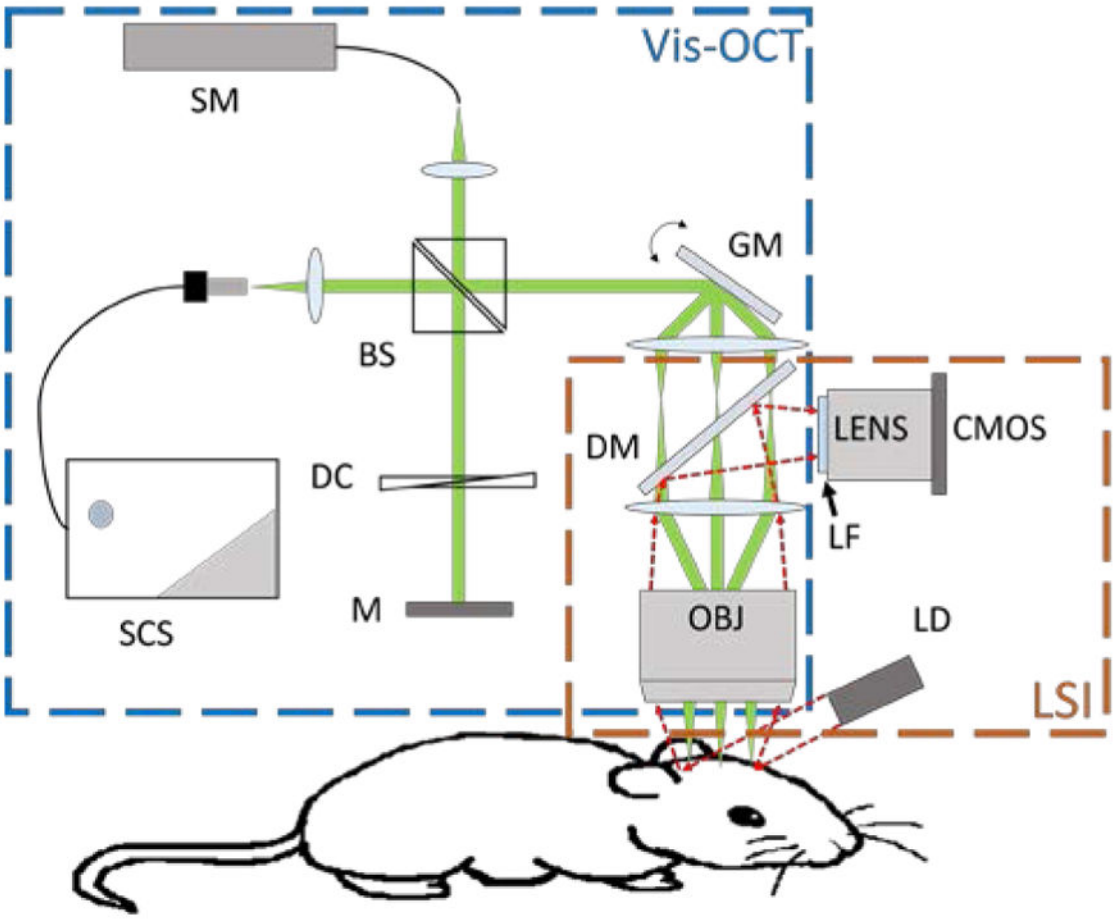

Fig. 1.

Schematic of the experimental system. SC: Supercontinuum source; SM: Spectrometer; BS: beam splitter; DC: dispersion compensation; M: mirror; GM: galvanometer mirrors; DM: dichroic mirror; LF: long-pass filter; OBJ: objective; LD: laser diode.

Author Manuscript Author Manuscript Author Manuscript Author Manuscript

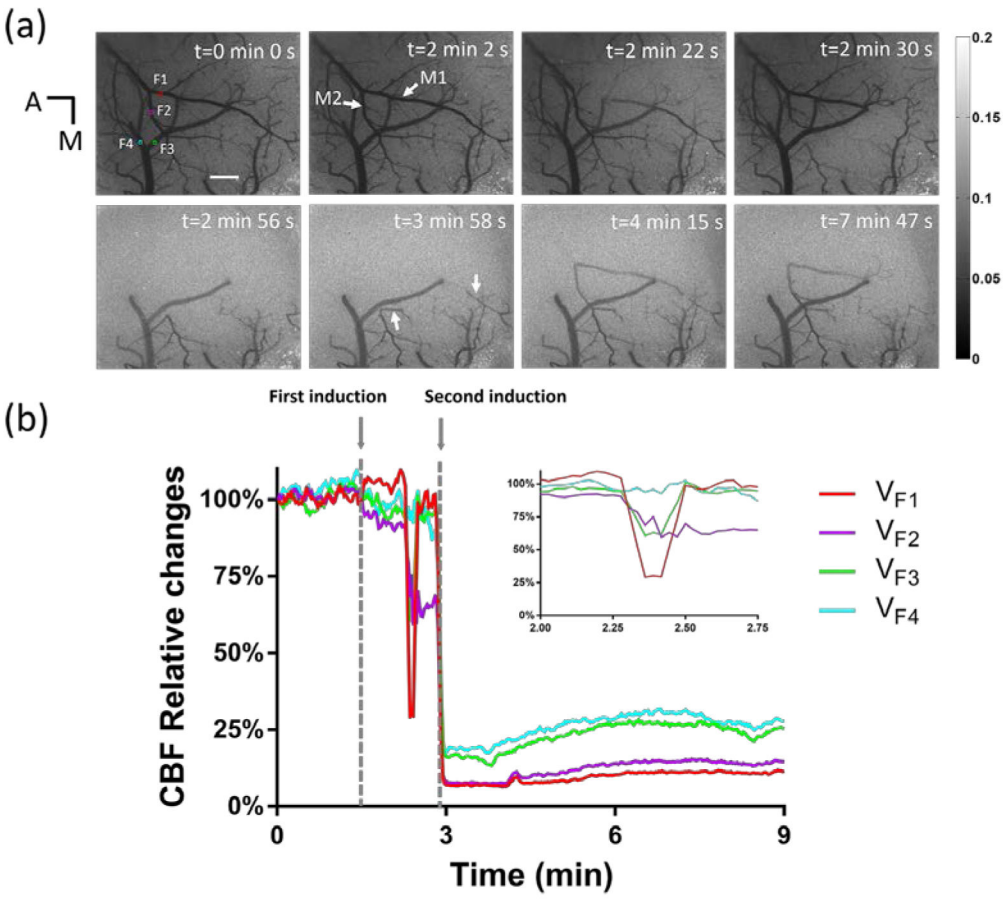

Fig. 2.

CBF changes before, during and after dMCAO induction. (a) LSI images at different time points. In Fig. 2(a) -0 min, four squares labeled with red, magenta, green and blue indicates area F1 and F2 on artery, and F3 and F4 on vein. A, anterior; M, median. (b) The relative CBF changes in areas F1, F2, F3 and F4. The enlarged image shows the detailed change of relative CBF changes between t = 2 min 0 sec and t = 2 min 45 sec. Scale bar: 500 μm.

Author Manuscript Author Manuscript Author Manuscript Author Manuscript

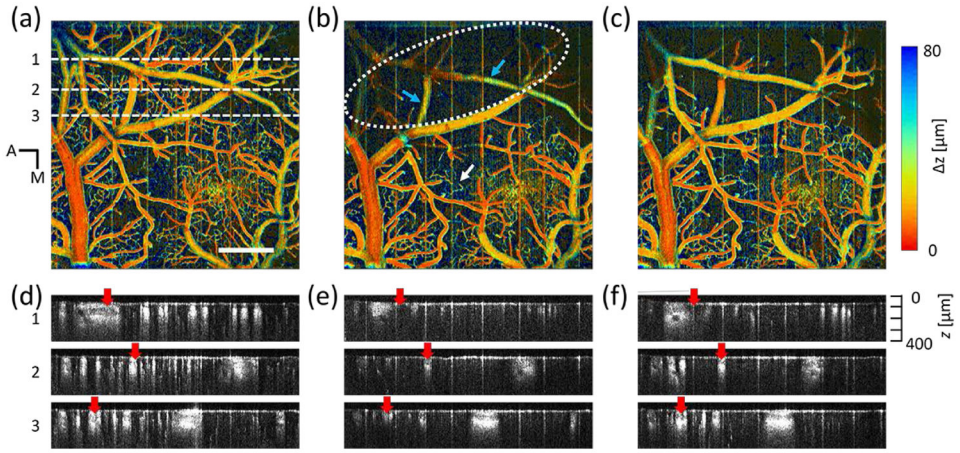

Fig. 3.

Depth-coded OCT angiograph in a mouse cortex. (a) Before the induction of dMCAO. (b) Immediately after the MCA occlusion. (c) After the reperfusion of MCA branch. Scale bar: 500 μm. (d), (e) and (f): OCTA B-scan images taken from (a), (b) and (c) at selected locations indicated by white dashed line in (a).

Author Manuscript Author Manuscript Author Manuscript Author Manuscript

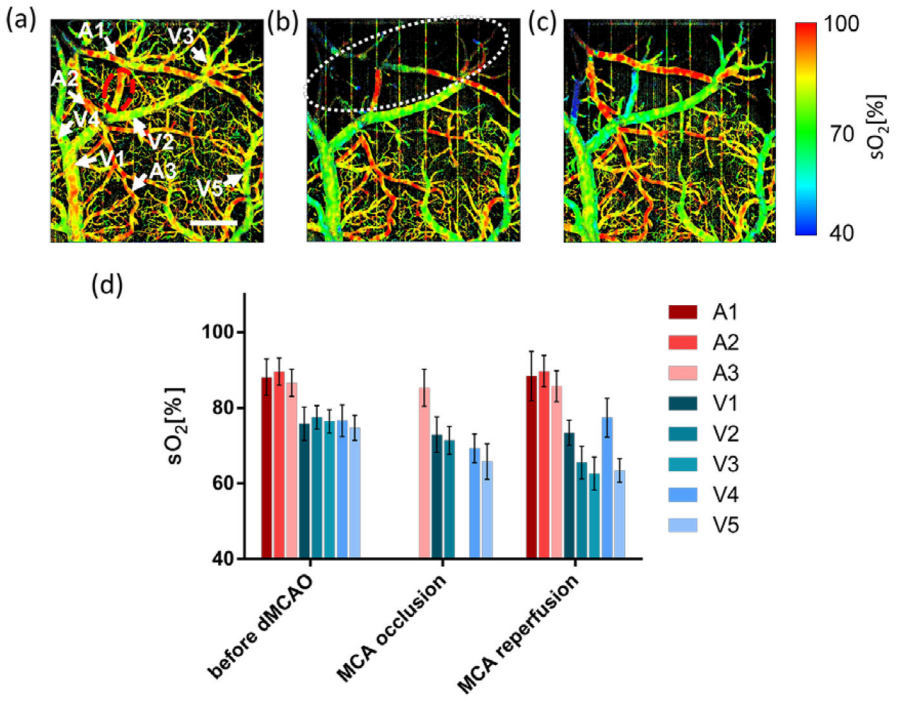

Fig. 4.

Vis-OCT angiography sO_2 map in a mouse cortex. (a) Before the induction of dMCAO. (b) Immediately after the MCA occlusion. (c) After the reperfusion of MCA branch. Scale bar: 500 μm. Arrows indicate the vessels where mean sO_2 was calculated. Dashed white line is the boundary of ischemic core area. Dashed red line is the area with overlapped arteries and veins. (d) Mean sO_2 values from the selected vessels. A1–A3 arteries and arterioles. V1–V5: veins and venules. Error bar: S.D.